

Diffusive high-temperature transport in the one-dimensional Hubbard model

Tomaž Prosen and Marko Žnidarič

Department of Physics, Faculty of Mathematics and Physics, University of Ljubljana, Ljubljana, Slovenia

(Dated: June 3, 2019)

We consider charge and spin transport in the one-dimensional Hubbard model at infinite temperature, half-filling and zero magnetization. Implementing matrix-product-operator simulations of the non-equilibrium steady states of boundary-driven open Hubbard chains for up to 100 sites we find clear evidence of diffusive transport for any (non-zero and finite) value of the interaction U .

PACS numbers: 71.27.+a, 05.70.Ln, 72.10.-d, 03.65.Yz

Introduction– The one-dimensional (1d) Hubbard model is the simplest model of strongly interacting dynamics of spinful fermions on a lattice within a single-band approximation. Its Hamiltonian reads

$$H = -t \sum_{i=1}^{L-1} \sum_{s \in \{\uparrow, \downarrow\}} (c_{i,s}^\dagger c_{i+1,s} + \text{h.c.}) + U \sum_{i=1}^L n_{i\uparrow} n_{i\downarrow}, \quad (1)$$

where the operators $c_{i,s}$, $c_{i,s}^\dagger$, for spin $s \in \{\uparrow, \downarrow\}$ and site $i \in \{1, \dots, L\}$ are standard fermionic annihilation and creation operators and $n_{i,s} := c_{i,s}^\dagger c_{i,s}$ are the density operators. The model is solvable by a coordinate Bethe ansatz [1] and possesses an infinite number of conservation laws [2]. While stationary properties of the 1d Hubbard model are well understood, see the monograph [3], much less is known about its dynamics, for instance about the transport behavior. In thermodynamically the most interesting regime, at half-filled band and zero magnetization $\sum_{i=1}^L \langle n_{i,s} \rangle = L/2$, studied in the present Letter, the model is gapped for charge excitations and gapless for spin excitations, for any $U \neq 0$. At zero temperature it is therefore an example of a Mott (charge) insulator and ballistic (ideal) spin conductor. Transport can be qualitatively characterized by a Drude weight – a linear response indicator of ballistic transport, defined as the weight of zero-frequency singular term $\delta(\omega)$ in the real part of conductivity $\sigma(\omega)$. Spin and charge Drude weights at zero temperature have been calculated in Ref. [4], with finite-size corrections given in [5], while a regular part of $\sigma(\omega)$ is studied in Ref. [6]. At nonzero temperature on the other hand no rigorous result is known and there is no consensus between numerical and Bethe ansatz based results. Thermodynamic Bethe ansatz suggests [7] that, even at half-filling, the charge Drude weight is finite, so the model was predicted to exhibit ideal charge transport; for a similar conclusion see also Quantum Monte Carlo calculation in Ref. [8]. Analytical calculations at large U on the other hand support vanishing charge Drude weight [9], for a study of low-energy excitations see also [10]. Exact numerical simulations of small systems, again at half-filling and at high/infinite temperature, suggest [11] $\sim 1/L$ scaling of the charge Drude weight. For temperatures much smaller than the gap semiclassical arguments to-

gether with field-theoretical scattering rate predicts diffusive transport [12]. Vanishing finite-temperature Drude weight in thermodynamic limit (TL) $L \rightarrow \infty$ offers the possibility of an insulating or diffusive behavior.

However, at high or infinite temperatures, non-equilibrium transport properties of 1d Hubbard model in either charge or spin sector are not known as there has been up to date no analytical or numerical method capable of reliably treating this regime. In this Letter we employ non-equilibrium steady state simulations [13] using an efficient matrix product ansatz [14] and provide a clear evidence of diffusive transport for both attractive $U < 0$ and repulsive $U > 0$ cases at infinite temperature. Namely, we show $1/L$ scaling of charge as well as of spin current and clear linear density profiles.

Boundary driven Hubbard chain– Using the Jordan-Wigner transformation we can map the 1d Hubbard model (1) to a spin-1/2 ladder system. Namely, writing $c_{i\uparrow} = P_{i-1}^{(\sigma)} \sigma_i^-$ where $P_i^{(\sigma)} = \sigma_1^z \cdots \sigma_i^z$ for spin-up fermions, and $c_{i\downarrow} = P_L^{(\sigma)} P_{i-1}^{(\tau)} \tau_i^-$ where $P_i^{(\tau)} = \tau_1^z \cdots \tau_i^z$ for spin-down fermions, one can verify that fermionic operators $c_{i,s}, c_{i,s}^\dagger$ satisfy canonical anticommutation relations provided σ_i^α and τ_i^α are two sets of Pauli matrices (and $\sigma_j^\pm := (\sigma_j^x \pm i\sigma_j^y)/2$, $\tau_j^\pm := (\tau_j^x \pm i\tau_j^y)/2$). Writing the Hubbard Hamiltonian (1) in spin-ladder form one obtains

$$H = -\frac{t}{2} \sum_{i=1}^{L-1} (\sigma_i^x \sigma_{i+1}^x + \sigma_i^y \sigma_{i+1}^y + \tau_i^x \tau_{i+1}^x + \tau_i^y \tau_{i+1}^y) + \frac{U}{4} \sum_{i=1}^L (\sigma_i^z + 1)(\tau_i^z + 1). \quad (2)$$

The spin-1/2 ladder system consists of two XX chains in two legs and a $Z-Z$ type interchain coupling along the rungs. For numerical simulations of the Hubbard model we shall use this ladder formulation (2).

To induce a nonequilibrium situation two legs are coupled to independent reservoirs. Their action is described in an effective way via the Lindblad equation [15] for the density matrix ρ of the ladder system,

$$\frac{d}{dt} \rho = i[\rho, H] + \mathcal{L}^{\text{dis}}(\rho), \quad (3)$$

where the dissipative term is expressed in terms of Lindblad operators L_k , as $\mathcal{L}^{\text{dis}}(\rho) =$

$\sum_k \left([L_k \rho, L_k^\dagger] + [L_k, \rho L_k^\dagger] \right)$. We use eight Lindblad operators acting locally on the first and last sites of each leg, injecting or absorbing fermions (spinons) with certain probability: $L_{1,2} = \sqrt{\Gamma(1 \mp \mu)} \sigma_1^\pm$, $L_{3,4} = \sqrt{\Gamma(1 \pm \mu)} \sigma_L^\pm$ for the first and $L_{5,6} = \sqrt{\Gamma(1 \mp \mu)} \tau_1^\pm$, $L_{7,8} = \sqrt{\Gamma(1 \pm \mu)} \tau_L^\pm$ for the second leg. Γ is the strength of the coupling to the baths while μ is a driving strength playing the role of a chemical potential bias. As demonstrated in previous studies of 1d spin chains [13] the precise form of Lindblad operators does not influence the bulk properties. Because of dissipative terms the time-dependent solution $\rho(t)$ of the Lindblad equation converges after long time to a time-independent state called a nonequilibrium steady state (NESS), $\rho_\infty = \lim_{t \rightarrow \infty} \rho(t)$, which is unique [16]. Once the steady state is reached, expressed in terms of a matrix product operator of a given bond dimension (following the method described in detail in Ref. [13] adapted for the spin ladder), expectation values of arbitrary observables in the NESS can be efficiently evaluated. All expectations given in this Letter are with respect to the NESS, that is $\langle A \rangle = \text{tr}(\rho_\infty A)$, which we will – when it is clear from the context, and to simplify notation – denote just by A . In each NESS calculation we have checked that the convergence is reached, i.e., we evolve the Lindblad equation (3) until a time-independent state is obtained, and that the results are stable with respect to increasing bond dimension [18]. For $\mu = 0$, i.e., no driving, one has an equilibrium setting, resulting in a trivial NESS $\rho_\infty \propto 1$. This means that for small driving μ we are studying nonequilibrium behavior at an infinite temperature. Note that such an infinite temperature state is separable in the operator space. Since the efficiency of the numerical method crucially depends on the entanglement infinite-temperature nonequilibrium states are the easiest ones to calculate because the entanglement is expected to be smaller than at finite temperatures.

Expectation values of fermionic observables are obtained from the corresponding ones in the ladder formulation, for instance, particle densities are $n_{i\uparrow} = (\sigma_i^z + 1)/2$ and $n_{i\downarrow} = (\tau_i^z + 1)/2$. Magnetization currents of two spin species, defined through continuity equations $d(\sigma_i^z/2)/dt = j_i^{(\sigma)} - j_{i-1}^{(\sigma)}$, $d(\tau_i^z/2)/dt = j_i^{(\tau)} - j_{i-1}^{(\tau)}$, are $j_i^{(\sigma)} = -\frac{t}{2}(\sigma_i^x \sigma_{i+1}^y - \sigma_i^y \sigma_{i+1}^x)$, $j_i^{(\tau)} = -\frac{t}{2}(\tau_i^x \tau_{i+1}^y - \tau_i^y \tau_{i+1}^x)$. In fermionic picture the particle (charge) current is $j_i^{(c)} = j_i^{(\sigma)} + j_i^{(\tau)}$, while the spin current is $j_i^{(s)} = (j_i^{(\sigma)} - j_i^{(\tau)})/2$. Particle density is $n_i = n_{i\uparrow} + n_{i\downarrow}$, while spin density is $s_i = (n_{i\uparrow} - n_{i\downarrow})/2$. Because of the same driving at both ladder legs the currents $j^{(\sigma)}$ and $j^{(\tau)}$ are the same. Therefore, NESS is such that it has a nonzero charge current and zero spin current. We have also performed simulations with Lindblad operators on the τ -chain driving transport in the opposite direction, that is with $L_{5,6} =$

$\sqrt{\Gamma(1 \pm \mu)} \tau_1^\pm$, $L_{7,8} = \sqrt{\Gamma(1 \mp \mu)} \tau_L^\pm$. In such a case the NESS has a nonzero spin current and zero charge current because $j^{(\tau)} = -j^{(\sigma)}$ holds. Results are practically the same as for the data presented, with the roles of $j^{(s)}$ and $j^{(c)}$ interchanged, meaning that the spin and charge transport behave in the same way at an infinite temperature. Furthermore, we stress that spin and charge transport are interchanged under the particle-hole transformation for the *down* spin fermions only, $R j_i^{(s)} R^\dagger = j_i^{(c)}/2$, which is defined as $R := \prod_{i=1}^L \tau_i^x = R^\dagger$ and flips the sign of interaction $RH(U)R^\dagger = H(-U)$, provided one takes a symmetric interaction term $(n_{i\uparrow} - \frac{1}{2})(n_{i\downarrow} - \frac{1}{2})$ in (1) or, equivalently, adds a chemical term $-UN/2$ to H with $N = \sum_{i,s} n_{i,s}$. Even though our master equation evolution (3) does not strictly conserve N , we have checked explicitly that the results based on Hamiltonians H and $H - UN/2$ are identical, so we conclude also that the infinite temperature transport characteristics of $H(U)$ and $H(-U)$ at half-filling are the same.

Results- We set $t = 1$, $\Gamma = 1$ and $\mu = 0.2$, except in Fig. 5 where $\mu = 1$. Driving $\mu = 0.2$ corresponds to equilibrium density in the reservoirs of $n_L = 0.4$ at the left end and $n_R = 0.6$ at the right end. The average filling ratio is therefore $n = 1/2$, $\sum_{i=1}^L n_{i\uparrow} = \sum_{i=1}^L n_{i\downarrow} = L/2$. The value $\mu = 0.2$ is at the upper end of a linear response regime. For large drivings $\mu \gtrsim 0.6$ one gets a negative differential conductance effect [19], where current decreases with increasing driving. The main goal of this Letter is to classify spin and charge transport, whether it is ballistic, diffusive or anomalous. For NESS different transport regimes are reflected in the scaling of the current on the system size. Fixing the driving strength μ , in a ballistic conductor the current is independent of system length, $j \sim L^0$, for a diffusive conductor it scales as $j \sim 1/L$, whereas in the anomalous case the current is proportional to a fractional power of L . We therefore calculated NESSs for different sizes L . Typical density profile is shown in Fig. 1. One can see that the densities of spin-up and spin-down fermions are linear in the bulk. Jumps in the density at the boundaries are due to oversimplified Lindblad operators that are not “matched” to the bulk dynamics, i.e., there are boundary resistances. Because these jumps are rather large we have fitted a linear function to the density profile in the bulk, thereby obtaining the density gradient $\nabla n_{i\uparrow} = \nabla n_{i\downarrow} = \nabla n_i/2$. In Fig. 2 we then plot the scaling of charge current (which is in the NESS independent of the site) with the gradient of charge density. At interaction $U = 1$ one can see a nice scaling $j^{(c)} \sim 1/L$. Together with a linear density profiles this is a clear indication of diffusive charge transport. As mentioned, for spin transport virtually the same behavior is obtained (data not shown). For $U = 2$ the scaling is not quite as good. It seems that for shorter chains $j^{(c)}$ decreases with L slower than $1/L$, however, for two largest sizes that we managed to cal-

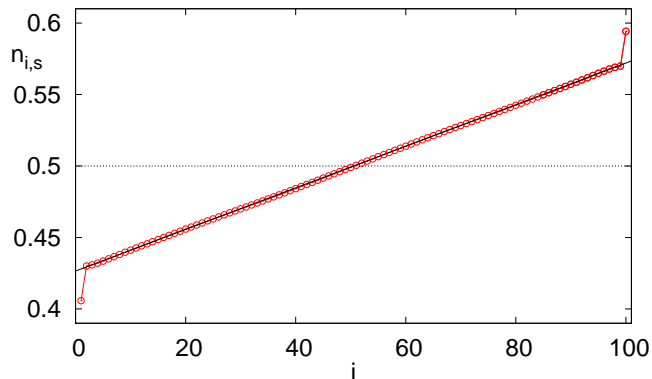


FIG. 1. (Color online) Density profile $n_{i,s}$ along the chain for $L = 100$, $U = 1$. Apart from jumps at the boundary, density is linear which is typical for diffusive conductors. Solid black line, overlapping with the numerical points, is a best-fitting linear function.

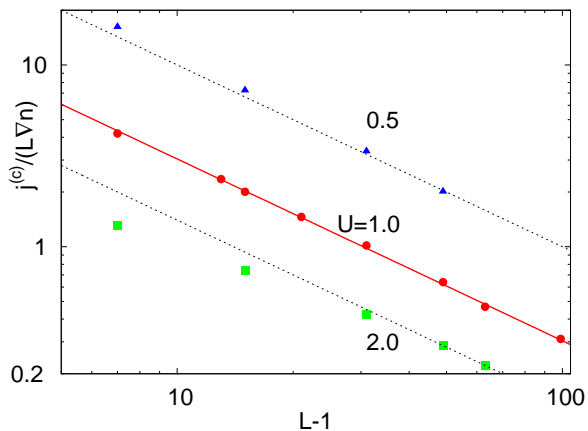


FIG. 2. (Color online) Scaling of charge current $j^{(c)}$ divided by the extrapolated density drop $L \nabla n$ with the system size L for different interactions U . Thick full (red) line, overlapping with $U = 1.0$ data, is $\sim 30.4/L$, indicating a diffusive transport. Two dashed lines also suggest $\sim 1/L$ scaling.

culate, a crossover to $\sim 1/L$ scaling is suggested. For smaller interaction $U = 0.5$ the situation seems similar. Looking at the density profiles at $U = 2$, shown in Fig. 3, which are linear in the bulk already for small sizes L , it seems natural to conjecture that the transport is diffusive in TL $L \rightarrow \infty$ for all nonzero finite values of U . Different transient scaling of the current with L for shorter chains is likely due to rather strong boundary effects. That the boundary effects are large can also be seen in the inset of Fig. 3(a), where we show the jump between the reservoir and the first site $n_{1\uparrow} - n_L$, as well as between the first two sites in the system $n_{2\uparrow} - n_{1\uparrow}$. While the boundary effects show a tendency to disappear in TL, at $U = 2$ and largest $L = 64$ they are still appreciable. One can try to optimize the coupling constant Γ in order to minimize the boundary effects, however we

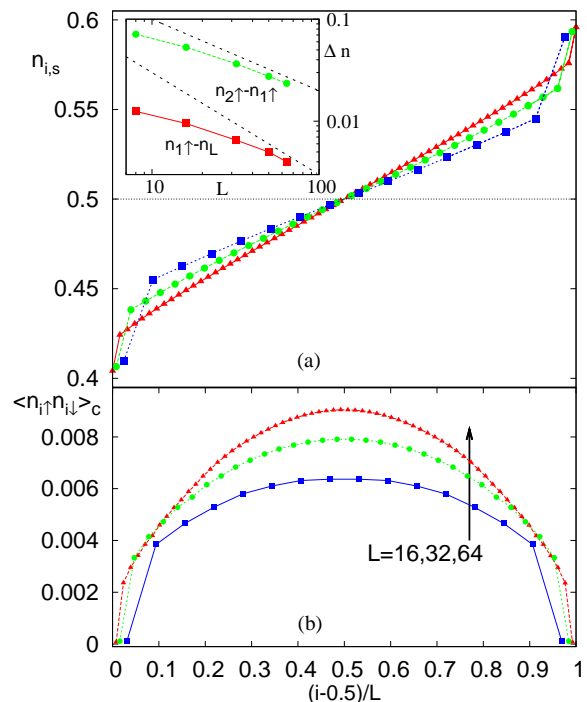


FIG. 3. (Color online) (a) Density profiles $n_{i,s}$ at $U = 2$, and (b) the corresponding connected density-density correlation function $\langle n_{i\uparrow} n_{i\downarrow} \rangle_c$. Data are shown for $L = 16$ (blue squares), $L = 32$ (green circles) and $L = 64$ (red triangles). Inset in (a): scaling of the jump between the reservoir and the 1st particle and between the 1st and 2nd particles, with size L . Black dashed lines indicate $\sim 1/L$ and $\sim 1/L^{0.7}$. Note that at $L = 64$ boundary jumps still account for around 25% of the total density difference between the chain ends.

found that $\Gamma \approx 1$ is usually close to the optimal value which does not seem to depend on L . In the Fig. 3(b) we show the connected spin-up spin-down correlation function $\langle n_{i\uparrow} n_{i\downarrow} \rangle_c = \langle n_{i\uparrow} n_{i\downarrow} \rangle - \langle n_{i\uparrow} \rangle \langle n_{i\downarrow} \rangle$, that gives on-site correlations between two fermion species. If we extrapolate our finite- L data to TL, we find $\langle n_{i\uparrow} n_{i\downarrow} \rangle_c \propto (\mu^2 - (2\langle n_{i\uparrow} \rangle - 1)(2\langle n_{i\downarrow} \rangle - 1))$, with a proportionality prefactor depending on U only, yielding a parabola for our linear density profiles. Interestingly, in the middle of the chain correlations become independent of the system size, while they are going to zero at the boundaries.

In the limit $U \rightarrow \infty$ the half-filled Hubbard model becomes equivalent to the 1d isotropic Heisenberg model. It has been found that at high temperature the isotropic Heisenberg model is an anomalous spin conductor, with the magnetization profiles having the arcsin-like shape [20]. That the same density profiles are obtained also in the Hubbard model at large U can be seen in Fig. 4. Fixing the length L and increasing U , density profiles become increasingly similar to the ones in the isotropic Heisenberg model. Isotropic Heisenberg model displays an anomalous transport with the magnetization current scaling as $\sim 1/\sqrt{L}$ [20] which can perhaps explain

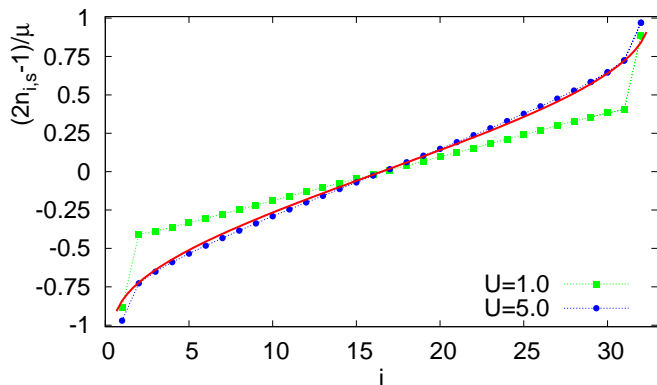


FIG. 4. (Color online) As one increases U at fixed length $L = 32$ the Hubbard model approaches the Heisenberg limit. Rescaled density profiles $(2n_{i,s} - 1)/\mu$, shown for $U = 1$ and $U = 5$ therefore become similar to $\frac{2}{\pi} \arcsin[\frac{2i-1}{L} - 1]$ (full red curve), found in the isotropic Heisenberg model [20].

slower decay of the current with L in the Hubbard model for small L 's and larger U , seen for instance in Fig. 2 at $U = 2$. Note that the limits $U \rightarrow \infty$ and $L \rightarrow \infty$ do not commute. In order to recover the Heisenberg behavior in TL one has to first let $U \rightarrow \infty$ and only then $L \rightarrow \infty$.

Finally, we briefly discuss the case of strong driving. We choose a maximal driving $\mu = 1$ and calculate the NESS. Density profile is shown in Fig. 5. We can see that the profile is in TL given by a simple cosine shape $n_{i,s} = \sin^2(\pi(2i - 1)/4L)$, exactly the same as has been found analytically in the isotropic Heisenberg model at strong driving [21]. This suggests that similar exact solution for NESS at maximum driving $\mu = 1$ as for the Heisenberg spin chain is also achievable for the Hubbard model and points to wider applicability of the algebraic method proposed in Refs. [21, 22].

Conclusion– Summarizing our findings about the transport in half-filled zero-magnetization 1d Hubbard model at an infinite temperature, we have shown that at finite interaction U both charge and spin transport are diffusive. This conclusion is based on the scaling of the currents with the system size for up to 100 particles, as well as on perfectly linear density profiles away from the boundaries. This complements ballistic spin transport at $U = 0$ and arbitrary temperature and anomalous transport at high temperature and $U = \infty$. We acknowledge support by the grants P1-0044 and J1-2208 of Slovenian Research Agency (ARRS).

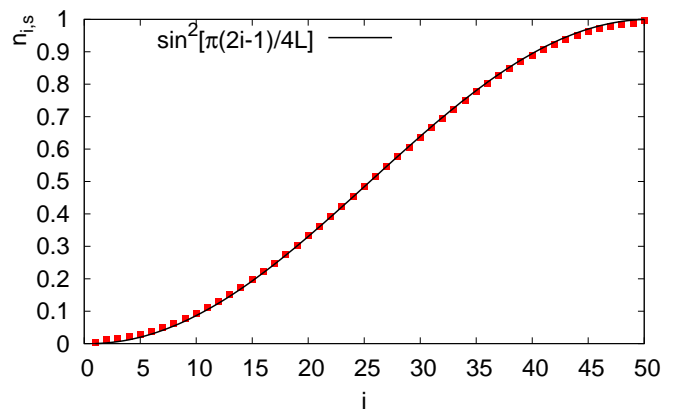


FIG. 5. (Color online) At maximal driving, $\mu = 1$, density profiles have a cosine shape (red squares, for $L = 50$, $U = 1$) while the current scales as $\sim 1/L^2$ (data not shown), exactly as in the Heisenberg model at maximal driving [21].

-
- [1] E. H. Lieb and F. Y. Wu, Phys. Rev. Lett. **20**, 1445 (1968); Physica A **321**, 1 (2003).
 [2] B. S. Shastry, Phys. Rev. Lett. **56**, 1529 (1986).
 [3] F. H. L. Essler, H. Frahm, F. Göhmann, A. Klümper, and V. E. Korepin, *The One-Dimensional Hubbard Model* (Cambridge, 2005).

- [4] B. S. Shastry and B. Sutherland, Phys. Rev. Lett. **65**, 243 (1990).
 [5] C. A. Stafford, A. J. Millis, and B. S. Shastry, Phys. Rev. B **43**, 660 (1991).
 [6] E. Jeckelmann, F. Gebhard, and F. H. L. Essler, Phys. Rev. Lett. **85**, 3910 (2000); R. M. Fye, M. J. Nartins, D. J. Scalapino, J. Wagner, and W. Hanke, Phys. Rev. B **44**, 6909 (1991).
 [7] S. Fujimoto and N. Kawakami, J. Phys. A **31**, 465 (1998).
 [8] S. Kirchner, H. G. Evertz, and W. Hanke, Phys. Rev. B **59**, 1825 (1999).
 [9] N. M. R. Peres, R. G. Dias, P. D. Sacramento, and J. M. P. Carmelo, Phys. Rev. B **61**, 5169 (2000).
 [10] S.-J. Gu, N. M. Peres, and J. M. P. Carmelo, J. Phys.: Condens. Matter **19**, 506203 (2007).
 [11] P. Prelovšek, S. El Shawish, X. Zotos, and M. Long, Phys. Rev. B **70**, 205129 (2004).
 [12] S. Sachdev and K. Damle, Phys. Rev. Lett. **78**, 943 (1997); K. Damle and S. Sachdev, Phys. Rev. Lett. **95**, 187201 (2005).
 [13] T. Prosen and M. Žnidarič, J. Stat. Mech. **2009**, P02035 (2009).
 [14] G. Vidal, Phys. Rev. Lett. **91**, 147902 (2003); F. Verstraete, J. J. Garcia-Ripoll, and J. I. Cirac, Phys. Rev. Lett. **93**, 207204 (2004); A. J. Daley, C. Kollath, U. Schollwöck, and G. Vidal, J. Stat. Mech. **2004**, P04005 (2004).
 [15] V. Gorini, A. Kossakowski, and E. C. G. Sudarshan, J. Math. Phys. **17**, 821 (1976); G. Lindblad, Comm. Math. Phys. **48**, 119 (1976).
 [16] NESS is in our case unique and is therefore reached irrespective of the initial state $\rho(0)$. Evans theorem [17] states that NESS (fixed point of a Liouvillian dynamical semi-group (3)) is unique iff the set of operators $\{H, L_1, L_2, \dots\}$, in our case $\{H, \sigma_{1,L}^\pm, \tau_{1,L}^\pm\}$, generates, under multiplication and addition, the entire algebra of operators, in our case over the spin ladder on L sites. Indeed, this can be verified by operator identities giving a recursive generation of σ_j^\pm : $\sigma_2^+ = (1/4)\sigma_1^+[\sigma_1^+, [H, \sigma_1^+]]$, and for $j \geq 2$, $\sigma_{j+1}^+ = -\sigma_{j-1}^+ - (1/2)\sigma_j^+[\sigma_j^-, \sigma_j^+ H \sigma_j^+]$. Operators for the second leg τ_j^\pm are generated through a

similar recursion, replacing σ_j^α by τ_j^α . Finally, all possible products of $\{\sigma_j^\pm\}$ and $\{\tau_j^\pm\}$ generate the entire operator algebra of the Hubbard chain.

- [17] D. E. Evans, *Comm. Math. Phys.* **54**, 293 (1977).
- [18] We use bond dimensions up to $D = 80$. Convergence times t_∞ typically scale $\propto L$, for example for $L = 100$ we needed to simulate (3) up to $t_\infty \approx 500$.
- [19] G. Benenti, G. Casati, T. Prosen, D. Rossini, and M. Žnidarič, *Phys. Rev. B* **80**, 035110 (2009).
- [20] M. Žnidarič, *Phys. Rev. Lett.* **106**, 220601 (2011); M. Žnidarič, *J. Stat. Mech.* **2011**, P12008 (2011).
- [21] T. Prosen, *Phys. Rev. Lett.* **107**, 137201 (2011).
- [22] T. Prosen, *Phys. Rev. Lett.* **106**, 217206 (2011).